DOI: 10.3901/CJME.2016.0324.037, available online at www.springerlink.com; www.cjmenet.com

# Theoretical Calculations and Experimental Verification for the Pumping Effect Caused by the Dynamic Micro-tapered Angle

CAI Yufei[1], ZHANG Jianhui[2, 3, *], ZHU Chunling[1], HUANG Jun[3, 4], and JIANG Feng[3]

1 *College of Aerospace Engineering, Nanjing University of Aeronautics and Astronautics, Nanjing 210016, China*
2 *School of Electro-Mechanical Engineering, Guangzhou University, Guangzhou 510006, China*
3 *State Key Laboratory of Mechanics and Control of Mechanical Structures, Nanjing University of Aeronautics and Astronautics, Nanjing 210016, China*
4 *Research Center of Fluid Machinery Engineering and Technology, Jiangsu University, Zhenjiang 212013, China*

Received August 26, 2015; revised January 26, 2016; accepted March 24, 2016

**Abstract:** The atomizer with micro cone apertures has advantages of ultra-fine atomized droplets, low power consumption and low temperature rise. The current research of this kind of atomizer mainly focuses on the performance and its application while there is less research of the principle of the atomization. Under the analysis of the dispenser and its micro-tapered aperture's deformation, the volume changes during the deformation and vibration of the micro-tapered aperture on the dispenser are calculated by coordinate transformation. Based on the characters of the flow resistance in a cone aperture, it is found that the dynamic cone angle results from periodical changes of the volume of the micro-tapered aperture of the atomizer and this change drives one-way flows. Besides, an experimental atomization platform is established to measure the atomization rates with different resonance frequencies of the cone aperture atomizer. The atomization performances of cone aperture and straight aperture atomizers are also measured. The experimental results show the existence of the pumping effect of the dynamic tapered angle. This effect is usually observed in industries that require low dispersion and micro- and nanoscale grain sizes, such as during production of high-pressure nozzles and inhalation therapy. Strategies to minimize the pumping effect of the dynamic cone angle or improve future designs are important concerns. This research proposes that dynamic micro-tapered angle is an important cause of atomization of the atomizer with micro cone apertures.

**Keywords:** atomization, nozzle/diffuser flow, dynamic cone angle, piezoelectric pump

## 1 Introduction

The applications of liquid atomization and ejection are widely found. As MEMS technology develops, the atomization field also develops with the trends to smaller droplet sizes and lower dispersion. This significantly improves the equipment for atomization inhalation therapy[1]. Food and Drug Administration's (FDA) guidance documents show that the mass median aerodynamic diameter (MMAD) of the drug particles produced by any inhalation equipment for bronchitis therapy should be less than 5 μm so as to give adequate therapy[2]. Besides the applications for inhalation therapy, the applications of ultra-fine atomized droplets are also widely found in the fields of printed circuits[3], 3D printing[4], precise surface coating[5–6], spray drying[7–10], fire suppression[11–14], electronic equipment cooling[15–18], and so on.

The traditional atomization methods generally include two: pneumatic atomization and ultrasonic atomization. Both these methods release energy to the liquid system to break the surface tension of the liquid and allow droplets to escape from the surface for atomization and ejection. Droplets are formed only on the surface but energy is applied to the entire liquid system. Hence, breaking the liquid into droplets and ejecting these particles are neither cost-effective nor energy-effective. Besides, the droplets are formed and ejected in a random and uncontrolled manner, which results in a wide range of droplet sizes.

To resolve the problems such as atomization rate not high enough, large droplet size range and low energy utilization, the atomizers with a plate which have micro apertures on it are used to eject the liquid through the micro apertures to form a spray. The introduction of micro apertures makes the atomization process more controllable. The atomizers with micro apertures are categorized into two based on whether the plate is vibrating during operations: vibratory micro-aperture atomizer and stationary micro-aperture atomizer.

In respect of stationary micro-aperture atomizers, HEIJ, et al[19–20], proposed a stationary micro-aperture atomizer driven by piezoelectricity in 1999. This atomizer consists of

*Corresponding author. E-mail: zhangjh@nuaa.edu.cn
Supported by National Natural Science Foundation of China (Grant Nos. 51375227, 91223201)

a sealed liquid chamber with micro apertures and a piezo actuator glued on the other side. When the diameter of its micro apertures is 5 μm and the driving frequency is between 250 and 300 kHz, the produced droplets come with an average diameter of 4.5 μm. In 2007, PAN, et al[21], designed a stationary micro-aperture atomizer with the micro aperture diameter of 8 μm and its operating power is about 1 W. When the operating frequency is 16 kHz, the atomization rate reaches 1.8 mL/min and the mass median diameter (MMD) of the droplets could be 6.13 μm. With the micro-aperture atomizer, the escaped droplets come with a smaller range of sizes and velocities than the traditional tools, but this atomizer could have a more complicated structure as it needs an atomization chamber with variable volume.

The vibratory micro-aperture atomizer investigated here combines the vibrators with micro apertures. The structure of this atomizer is simple because it doesn't need the atomization chamber which has variable volume. Besides, it benefits from the same controllable atomization process with the atomizer discussed above. In 1986, MAEHARA, et al[22–23], first proposed the atomizer with this structure and improved the structure. SHEN, et al[24–25], improved the dispenser by replacing with a cymbal-shaped powerful dispenser. Under a frequency of 127.89 kHz and an atomizer rate of 0.5 mL/min, the atomizer designed by SHEN, et al is able to produce the droplets with a MMAD of 4.07 μm. This atomizer can operate with high viscosity fluids (cP>3.5) and deliver high quality atomization of them with only about 1.2 W consumption. Perfect to the portable atomization inhabitation therapy, this atomizer brings a lot of benefits such as easy operations and its small size.

Several difficulties prevent further reduction of the droplet size and its range. These difficulties are attributed to how the micro-tapered aperture atomizer works.

## 2 Review on the Structure and Principle of Atomizers

Fig. 1 shows the schematic structure of the micro-tapered aperture atomizer device. This device consists of an atomizer and a water tank. The atomizer consists of a piezoceramic ring and a dispenser which is a stainless steel sheet with micro-tapered apertures. When driven by the high-frequency vibrations of the piezoceramic ring, the dispenser is also vibrating, which allows ejection and atomization.

For how this atomizer works, MAEHARA, et al[22–23], suggested that the sound pressure generated in the liquid which is caused by the vibrations of the dispenser results in atomization. LU, et al[15, 26], suggested that the efficiency of the dispenser pumping mechanism depends on the balance between inertial and capillary forces; when the dispenser moves to the flared side, the liquid is pinched off as droplets passing through the cone nozzle; when the dispenser moves the tapered side, the liquid adheres to the orifice through capillary force.

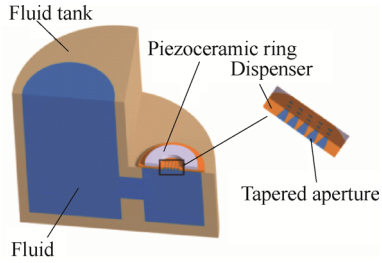


Fig. 1. Illustration of the atomizer structure

All the above suggestions don't include the contributions of cone apertures to atomization. The aim of this paper is to investigate the dynamic cone angle phenomenon during vibrations and analyze its pumping effect on the liquid as well as to prove it helps to dispenser's pumping and atomization effect.

## 3 Dispenser Vibrations

### 3.1 Deformation of micro-tapered apertures

The dispenser is deformed as driven by the piezoceramic ring. Its deformation also results in the deformation of cone apertures in the dispenser. Calculating the deformation of cone apertures is necessary to investigate the atomization from the dispenser. Hence, in order to calculate the deformation of cone apertures when the dispenser is vibrating, the following conditions are assumed:

(1) When the dispenser is vibrating in the upward and downward directions, the deformation and velocity are symmetrical with respect to the original neutral surface.

(2) The dispenser vibrations meet the Kirchhoff hypothesis.

The coordinate system is created with above assumptions, the neutral surface of the dispenser is $xy$ plane and the $z$ axial is perpendicular to it, as shown in Fig. 2(a). In order to illustrate the deformation of the apertures easily, the $xz$ plane is shown in Fig. 2(b). According to Kirchhoff hypothesis, there is no movement of the dispenser neutral surface in $x$ and $y$ directions. Any straight line which is vertical to the neutral surface before its deformation is still vertical to the elastic and flexible plane after its deformation. The length of the line remains the same. If the neutral surface is $z=f(x, y)$ after its deformation, the movement from $P$ to $P'$ on the dispenser is shown in Fig. 2(c), where $PP_0$ is perpendicular to $xy$ plane and $P'P_0'$ is perpendicular to the surface $f(x, y)$.

According to Kirchhoff hypothesis, the point $P_0(x_0, y_0, 0)$ changes to $P_0'[x_0, y_0, f(x_0, y_0)]$ after the deformation. Eq. (1) is to calculate the normal at $P_0'$ on the neutral surface after the deformation, where $f_x$ and $f_y$ respectively refer to the partial derivatives of $f(x, y)$ at $x_0$ and $y_0$:

$$\begin{cases} x - x_0 = f_x[z - f(x_0, y_0)], \\ y - y_0 = f_y[z - f(x_0, y_0)]. \end{cases} \tag{1}$$

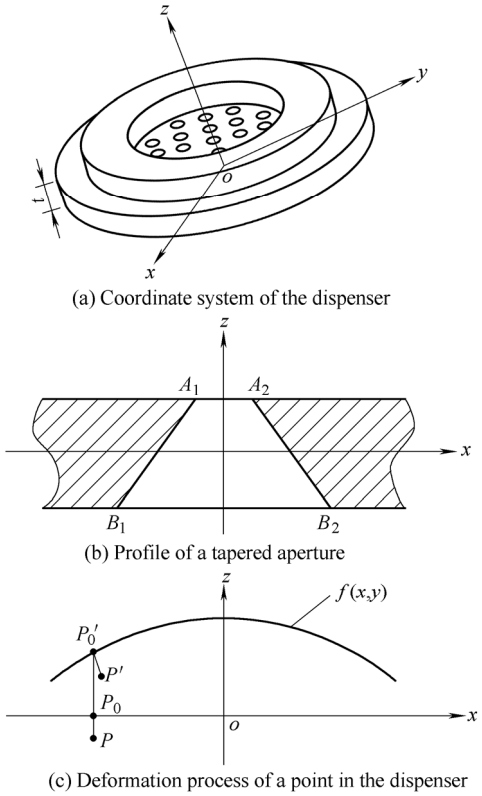


Fig. 2. Schematic coordinate of the dispenser

Before the deformation, the distance between $P$ and $P_0$ is $|z_0|$. With $|PP_0|=|P'P_0'|$ which is obtained from Kirchhoff hypothesis, following equation results:

$$\sqrt{(x_0-x_0')^2+(y_0-y_0')^2+(f(x_0,y_0)-z_0')^2}=|z_0|. \quad (2)$$

The coordinate of $P'$ is calculated with Eq. (1) and Eq. (2), and the result is $(x_0-af_x, y_0-af_y, a+f)$, where $a=z_0\Big/\sqrt{1+f_x^2+f_y^2}$.

### 3.2 Volume changes of micro-tapered apertures

Using the effect of $d_{31}$ piezoceramic ring, the vibration is stimulated, and then the elastic deformations of the metal sheets at the upper and lower sides of the neutral surface are generated. The metal sheets at both sides of the neutral surface are stretched or compressed. The direction where the metal sheet stretches is opposite against the direction where it compresses. Fig. 3 illustrates the highest and lowest positions of a micro-tapered aperture in a cycle.

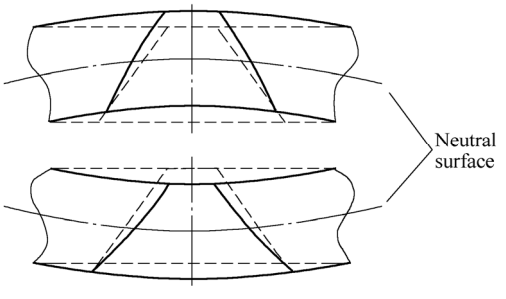


Fig. 3. Deformation occurs when a single cone aperture is vibrating in the upward and downward directions

When driven by periodic excited vibrations, a point on the non-neutral surface moves in two available cycles: 1) stretched from equilibrium to its limit, released back to equilibrium, compressed from equilibrium to its limit, and then released back to equilibrium; or 2) compressed from equilibrium to its limit, released back to equilibrium, stretched from equilibrium to its limit, and then released back to equilibrium. The cycle does not stop as the piezoceramic ring continues to deliver excitation. During the cycle, the micro-tapered aperture volume varies with the changes in the cone angle.

The fluid flow in the micro-tapered aperture is closely connected with its volume changes. In order to find out the flow in this aperture, its volume changes must be calculated first. The surface equation for a micro-tapered aperture is shown as Eq. (3), where $\theta$ is the half angle of an aperture and $r_m$ is the diameter of the circle on its neutral surface. In order to calculate the entire volume changes of an aperture, it's necessary to calculate the volume changes of its micro unit. There is a micro unit at point $(x, y, z)$. Its dimensions are $\Delta x$, $\Delta y$ and $\Delta z$ and its volume before the deformation is $\Delta x\Delta y\Delta z$. The coordinates of the points $(x+\Delta x, y, z)$, $(x, y+\Delta y, z)$ and $(x, y, z+\Delta z)$ after the deformation can be obtained with the point deformation equation. With the second order Taylor expansion of the function at $(x, y, z)$ and the ignorance of the infinitesimal of high order, the vectors of the three sides of the micro unit at the top after the deformation can be calculated (see Eq. (4)):

$$\sqrt{x^2+y^2}=-\tan\theta\cdot z+r_m, \quad (3)$$

$$\begin{cases}\boldsymbol{v}_x=[\Delta x-af_{xx}\Delta x-a_xf_x\Delta x,\\ \qquad -af_{yx}\Delta x-a_xf_y\Delta x, a_x\Delta x+f_x\Delta x],\\ \boldsymbol{v}_y=[-af_{xy}\Delta y-a_yf_x\Delta y,\\ \qquad \Delta y-af_{yy}\Delta y-a_yf_y\Delta y, a_y\Delta y+f_y\Delta y],\\ \boldsymbol{v}_z=[-a_zf_x\Delta z,-a_zf_y\Delta z, a_z\Delta z].\end{cases} \quad (4)$$

The volume of its micro unit after the deformation can be obtained through the determinant composed of the three vectors $\boldsymbol{v}_x$, $\boldsymbol{v}_y$ and $\boldsymbol{v}_z$. As shown in Fig. 3, the aperture volume becomes smaller when the dispenser is vibrating in the upward direction and becomes larger when the dispenser is vibrating in the downward direction. The dispenser is vibrating symmetrically to the original neutral surface. Hence, If the function of the neutral surface is $f(x, y)$ when the dispenser reaches the highest position during vibrations, the function of the neutral surface is $-f(x, y)$ when the dispenser reaches the lowest position during vibrations. Eq. (5) and Eq. (6) respectively calculate the volumes of a cone aperture when the dispenser reaches the highest and lowest positions during vibrations. In these equations, $s=1+f_x^2+f_y^2+f_z^2$. The maximum change (Eq. (7)) of the cone aperture volume during vibrations can be obtained with Eq. (6) minus Eq. (5):

$$V_{\text{up}}=\iiint_{\Omega}[\sqrt{s}+z^2(f_{xx}f_{yy}-f_{xy}^2)s^{-3/2}+ z(-f_{yy}-f_{xx}-f_y^2f_{xx}+2f_xf_yf_{xy}-f_x^2f_{yy})s^{-1}]\mathrm{d}V, \quad (5)$$

$$V_{\text{dowm}}=\iiint_{\Omega}[\sqrt{s}+z^2(f_{xx}f_{yy}-f_{xy}^2)s^{-3/2}+ z(f_{yy}+f_{xx}+f_y^2f_{xx}-2f_xf_yf_{xy}+f_x^2f_{yy})s^{-1}]\mathrm{d}V, \quad (6)$$

$$\Delta V=\iiint_{\Omega}[2z(f_{yy}+f_{xx}+f_y^2f_{xx}- 2f_xf_yf_{xy}+f_x^2f_{yy})s^{-1}]\mathrm{d}V. \quad (7)$$

## 4 Flow Analysis

### 4.1 Flow resistance

With the cone aperture volume changes, there are flows inward to or outward from the aperture. The inward and outward flows are closely related with the flow resistance coefficient which is defined as follows:

$$k=\frac{\Delta p}{\frac{1}{2}\rho v^2}, \quad (8)$$

where $\rho$ is the density of the fluid, $v$ is the average velocity of the fluid, $\Delta p$ is the pressure drop.

As the sectional area of the cone aperture in $z$ direction is not consistent, the velocity of the fluid also changes when it is flowing. For easy calculation, the velocity of the flows at the neutral surface is considered as a reference here, and the pressure loss coefficient $\xi$ is introduced here. The pressure loss coefficient $\xi$ is defined as follows:

$$\xi=\frac{\Delta p}{\frac{1}{2}\rho v_{\text{m}}^2}, \quad (9)$$

where $v_{\text{m}}$ is the average velocity of the flows at the neutral surface.

The relation between the pressure loss and resistance coefficients is shown in Eq. (10), where $A_m$ is the sectional area of a cone aperture at the neutral surface and $A$ is the sectional area where actual flows start:

$$\xi=\left(\frac{A_{\text{m}}}{A}\right)^2 k. \quad (10)$$

The sectional area of a cone aperture and its resistance coefficient keep changing during dispenser vibrations. For easy calculation, the average area during the vibrations (i.e., the sectional area when it is static) is used for calculations in this paper. The sectional areas of the cone apertures at $A_1A_2$ and $B_1B_2$ are $A_{\text{A}}$ and $A_{\text{B}}$ respectively. $R_{\text{A}}=(A_{\text{m}}/A_{\text{A}})^2$ and $R_{\text{B}}=(A_{\text{m}}/A_{\text{B}})^2$ are defined here. The flow resistance in a cone aperture involves: the loss due to the local resistance when there are flows inward to or outward from it and the loss when the fluid flows through the diffuser or nozzle element. Because the shape of the cone aperture changes when the dispenser is vibrating, the average resistance coefficient value is used for calculations. When the volume of a cone aperture decreases, the fluid in it flows toward both sides and its flow resistance consists of the on-way resistance from the aperture and the local resistance for outflows. The pressure lost coefficients can be calculated with

$$\begin{aligned}\xi_{\text{Aout}}&=k_{\text{out}}R_{\text{A}}+k_{\text{An}},\\ \xi_{\text{Bout}}&=k_{\text{out}}R_{\text{B}}+k_{\text{Bd}}.\end{aligned} \quad (11)$$

Likewise, the pressure lost coefficient found when the fluid flows toward the cone aperture can be calculated with

$$\begin{aligned}\xi_{\text{Ain}}&=(k_{\text{in}}+k_{\text{Ad}})R_{\text{A}},\\ \xi_{\text{Bin}}&=(k_{\text{in}}+k_{\text{Bn}})R_{\text{B}}.\end{aligned} \quad (12)$$

Based on the equation for the equivalent pressure lost coefficient, the volume rate of the flows in or out of the cone aperture can be calculated:

$$q_{\text{V}}=\sqrt{\frac{2\Delta p}{\rho\xi}}A_{\text{m}}. \quad (13)$$

### 4.2 Flows driven by the dynamic cone angle

When the dispenser vibrates upward, the volume of the cone aperture decreases and the fluid in the aperture flows out through the two sides. The decreased volume is equal to the amount of fluid that flows out. In order to calculate the fluid flows caused by the changes of the aperture, the fluid pressure changes in the liquid chamber are ignored and the pressure at both sides of the dispenser is assumed to be the same. The relationship between variables of volume and flow resistance is obtained:

$$\Delta V=\left(\sqrt{\frac{2\Delta p_{\text{out}}}{\rho\xi_{\text{Aout}}}}+\sqrt{\frac{2\Delta p_{\text{out}}}{\rho\xi_{\text{Bout}}}}\right)\frac{A_{\text{m}}T}{2}, \quad (14)$$

where $T$ is the vibration cycle of the dispenser.

When the dispenser vibrates downward, the volume of the cone aperture increases and the fluid flows toward the aperture. The volume increase is equal to the amount of inflows:

$$\Delta V=\left(\sqrt{\frac{2\Delta p_{\text{in}}}{\rho\xi_{\text{in}}}}+\sqrt{\frac{2\Delta p_{\text{in}}}{\rho\xi_{\text{Bin}}}}\right)\frac{A_{\text{m}}T}{2}. \quad (15)$$

When $\Delta p_{\text{in}}$ and $\Delta p_{\text{out}}$ are calculated with Eq. (14) and Eq.

(15) respectively, the volume of the flows out of $A_1A_2$ during a cycle and the resulted volume rate can be obtained as follows:

$$V_{\text{net}} = \frac{\sqrt{\xi_{\text{Ain}}\xi_{\text{Bout}}} - \sqrt{\xi_{\text{Aout}}\xi_{\text{Bin}}}}{\left(\sqrt{\xi_{\text{Ain}}} + \sqrt{\xi_{\text{Bout}}}\right)\left(\sqrt{\xi_{\text{Aout}}} + \sqrt{\xi_{\text{Bin}}}\right)}\Delta V, \quad (16)$$

$$q_{Va} = nfV_{\text{net}}, \quad (17)$$

where $n$ is the number of apertures and $f$ is the vibration frequency. As the denominator in Eq. (16) is greater than zero, the direction of the macroscopic flow is determined by whether the numerator is positive or negative. When $V_{\text{net}}>0$, the macroscopic flow is from $B_1B_2$ to $A_1A_2$; when $V_{\text{net}}<0$, the macroscopic flow is from $A_1A_2$ to $B_1B_2$; when $V_{\text{net}}=0$, the macroscopic flow is 0, which means the deformation of the micro-tapered aperture cannot result in atomization. For the attribute of being positive or negative, $\sqrt{\xi_{\text{Ain}}\xi_{\text{Bout}}} - \sqrt{\xi_{\text{Aout}}\xi_{\text{Bin}}}$ is in consistent with $\xi_{\text{Ain}}\xi_{\text{Bout}} - \xi_{\text{Aout}}\xi_{\text{Bin}}$. $\xi_{\text{Ain}}\xi_{\text{Bout}} - \xi_{\text{Aout}}\xi_{\text{Bin}}$ can be calculated as follows:

$$\xi_{\text{Ain}}\xi_{\text{Bout}} - \xi_{\text{Aout}}\xi_{\text{Bin}} = R_{\text{A}}R_{\text{B}}k_{\text{out}}(k_{\text{Ad}} - k_{\text{Bn}}) + k_{\text{in}}(R_{\text{A}}k_{\text{Bd}} - R_{\text{B}}k_{\text{An}}) + (R_{\text{A}}k_{\text{Ad}}k_{\text{Bd}} - R_{\text{B}}k_{\text{An}}k_{\text{Bn}}). \quad (18)$$

Eq. (18) shows that whether it is positive or negative is not determined by the values of $k_{\text{out}}$ and $k_{\text{in}}$ but the difference between $k_{\text{Ad}}$ and $k_{\text{Bn}}$ and the difference between $k_{\text{Bd}}/R_{\text{B}}$ and $k_{\text{An}}/R_{\text{A}}$. Fig. 4 shows the flow resistances in the diffuser element[27]. When its cone angle is about 5°, the flow resistance coefficient reaches the minimum of about 0.13. The flow resistance in the nozzle element is much smaller. When the cone angle is 30°, the flow resistance coefficient is 0.02; when the angle reaches 60°, the flow resistance coefficient is only 0.07. OLSSON[28] made a comparison between the result obtained from the numerical calculation for conical flows and the result mentioned in Ref. [27] and it is found that the characterizes of the flow resistances in the nozzle/diffuser elements at a micro-size level are similar to those at a normal-size level. Hence, $k_{\text{Ad}}>k_{\text{Bn}}$, $k_{\text{Bd}}>k_{\text{An}}$, and also $R_{\text{A}}k_{\text{Bd}}>R_{\text{B}}k_{\text{An}}$ because of $R_B<R_A$. From the analysis above, the conclusion that $\Delta V>0$ is obtained. In a complete vibration cycle, the macroscopic flows from $B_1B_2$ to $A_1A_2$ are generated in the cone aperture.

If the apertures in the dispenser are straight, $R_{\text{A}}=R_{\text{B}}=1$ and $k_{\text{Ad}}=k_{\text{An}}=k_{\text{Bn}}=k_{\text{Bd}}$. Likewise, when $V_{\text{net}}=0$, the net flow in the apertures is 0 during a complete vibration cycle, which means there is no flow.

The volume changes of the micro-tapered aperture when the dispenser is vibrating and the difference between the flow resistances in the nozzle and diffuser elements make the micro-tapered aperture dynamic; this phenomenon is called a dynamic cone angle. It can be seen from the above discussions that the dynamic cone angle is capable to drive one-way flows directly, and the dynamic cone angle works as a pump.

### 4.3 Flows driven by the volume changes of liquid chamber

When the dispenser is vibrating, the volume of the cone aperture changes and the volume of the liquid chamber also changes because of the deformation of the dispenser. The way that these flows are produced is how the conical-flow valveless piezoelectric pump works. When the cone angle is small, the flow resistance in the diffuser element is less than it in the nozzle element. As the angle of the cone aperture increases, the boundary layer separation happens in the diffuser element and its resistance increases significantly, but the flow resistance in the nozzle element increases in a small amount (Fig. 4). Hence, when the angle of the cone aperture increases to a particular value, the flow resistance in the nozzle element becomes smaller than it in the diffuser element. Fig. 5[29] shows the relations between the cone aperture pressure lost coefficient and the angle, both of which are obtained from the test.

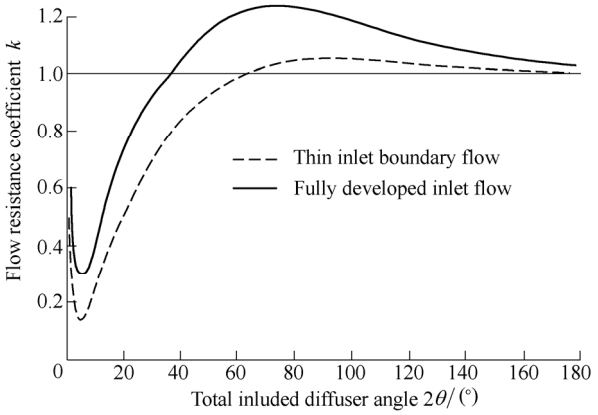


Fig. 4. Curves of the flow resistance coefficients of a diffuser element

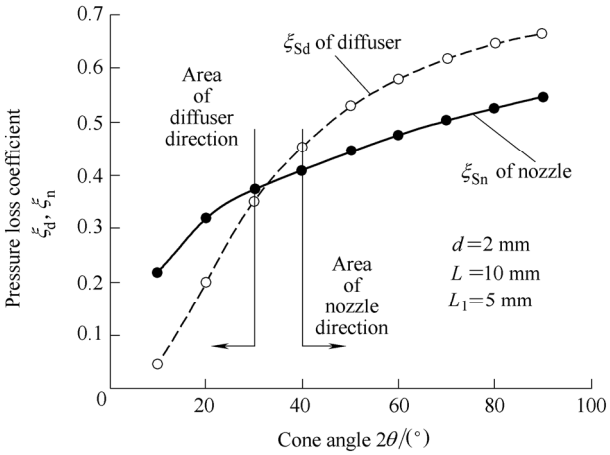


Fig. 5. Pressure loss coefficient curves created with the experiment on the flows in the nozzle and diffuser elements

Fig. 5 shows that when the angle of the cone aperture is greater than 35°, the flow resistance in the diffuser element is higher than it in the nozzle element. In this way, a

one-way flow can be produced after a complete cycle. The volume rate that is driven by the changes of the liquid chamber volume can be calculated with Eq. (19)[29]:

$$q_{Vc} \approx \Delta V_c f \frac{\xi_d - \xi_n}{\xi_d + \xi_n}, \tag{19}$$

where $\Delta V_c$ is the changes of the liquid chamber volume, and $\xi_d$ and $\xi_n$ are the flow resistance coefficients in the diffuser and nozzle elements respectively. With the volume changes of the cone aperture and liquid chamber, the overall volume rate can be calculated as follows:

$$q_V = q_{Va} + q_{Vc}. \tag{20}$$

## 5 Results and Experimental Validation

### 5.1 Dynamic cone angle pumping effect calculation

Following calculations and tests are carried out for the atomizer with straight apertures and the atomizer with cone apertures. The specific parameters of these atomizers are shown in Table 1. Fig. 6 shows the micro-tapered apertures photographed by a microscope.

**Table 1. Geometric parameters of the atomizer**

| Atomizer parameter | Value |
|---|---|
| Outer diameter of the piezoelectric ceramic ring $d_{out}$/mm | 16 |
| Inner diameter of the piezoelectric ceramic ring $d_{in}$/mm | 8 |
| Thickness of the piezoelectric ceramic ring $t_p$/mm | 1 |
| Diameter of the dispenser $d_d$/mm | 20 |
| Thickness of the dispenser $t$/μm | 100 |
| Diameter of straight apertures $d_s$/μm | 100 |
| Large diameter of cone apertures $d_{large}$/μm | 110 |
| Small diameter of cone apertures $d_{small}$/μm | 7 |

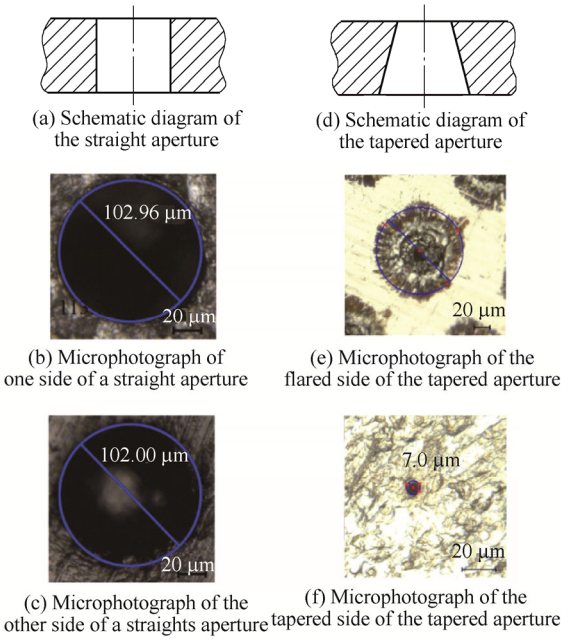


Fig. 6. Straight apertures and cone apertures photographed by KEYENCE VHX-1000

In order to investigate how the angle of a micro-tapered aperture impacts on the atomizer rate, Eq. (16) is used here to calculate the net flow from $A_1A_2$ surface during a vibrating cycle when the cone angle is changing from 5° to 60° and the diameter of neutral surface of the micro-tapered aperture is 58.5 μm. Fig. 7 shows the result. As shown in the figure, the net flow is increasing and then decreasing as the angle of the cone aperture is becoming larger. The main reason for its increase is that the flow resistant in the diffuser element increases as the angle increases and this allows the difference shown in the numerator of Eq. (16) to increase as well. The net flow rate reaches the maximum at about 24° and then decreases to about 0. The main reason of its decrease is that $R_A$ value increases as the angle increases and this allows the denominator of Eq. (16) to increase as well.

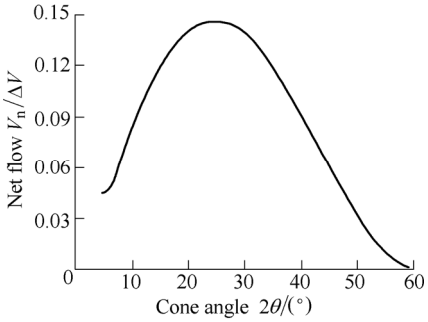


Fig. 7. Net flows caused by the dynamic cone angle effect during a vibrating cycle

### 5.2 Experimental validation

To validate the principle, two tests are carried out. First, followings are determined at 5–200 kHz by a laser vibrometer (PSV-300F): resonance points, vibration mode diagrams and the atomizer rates under the resonance frequencies. The structure of the atomizer device to be measured is illustrated in Fig. 8(a). It consists of a water tank and an atomizer, with the flared side of the dispenser in contact with the water. Figs. 9(a)–9(e) shows the resonance frequencies and their vibration modes. It also illustrates that the dispenser is deformed in a more complex way as the resonance frequency increases. Fig. 9(f) shows the atomizer rates under the resonance points found when the peak-to-peak voltage is 50 V and that when the frequency is 9.44 kHz or 21.58 kHz, the atomizer cannot produce effective atomization with only drops formed on the dispenser.

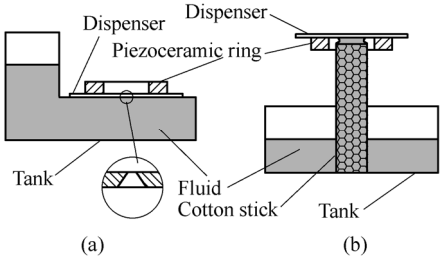


Fig. 8. Schematic equipment for the experiment

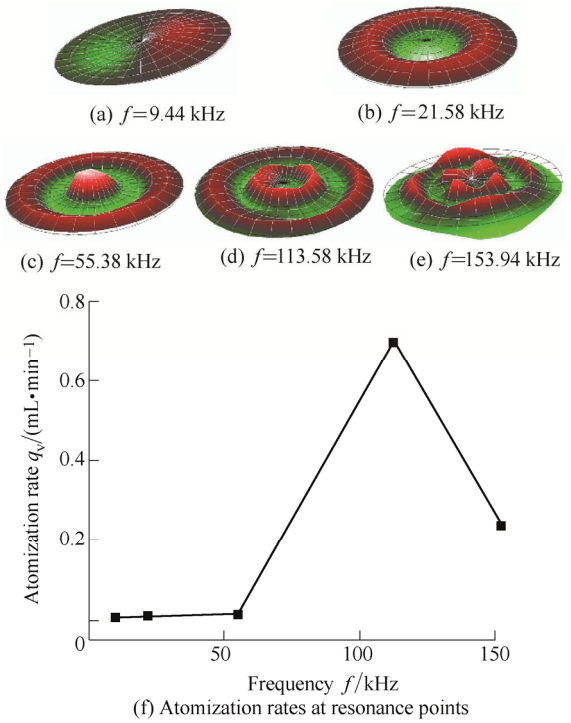


Fig. 9. Experimental results for the cone aperture dispenser

Fig. 9 shows that dispenser is deformed in a more complex way as the frequency increases, which means the deformation curvature also increases. However, the vibration amplitude decreases as the resonance frequency increases, which allows the volume changing rate of the water tank to decrease, but the atomizer rate under the resonant frequency generally increases incrementally. This finding disagrees with previous discussions on the pumping effect caused by volume changes of the water tank as well as the atomization generated under ultrasound conditions. However, the dynamic cone angle shown in Fig. 3 has larger changes as the changing rate of the dispenser deformation curvature increases. Eq. (7) shows that the volume changing rate of a micro-tapered aperture increases as the changing rate of the deformation curvature increases. This allows the dynamic cone angle pumping effect calculated with Eq. (16) to become stronger and so the atomizer rate also increases. Hence, the vibration and elastic deformation of the dispenser allow the micro-dynamic cone angle to work as a pump. There are two possible reasons for the reduction of the atomization rate when the frequency reaches 153.94 kHz. The first is that the overall displacement amplitude decreases at higher resonance modes and the rate of change also decreases. The second reason is that the flow velocity in the aperture increases with increasing frequency, and this leads to the increased flow resistance.

The atomizer rates are measured when the atomizer is in the forward and reverse directions (defined in Fig. 10 and Fig. 11). Because the atomizer rates under both forward and reverse directions need to be measured, the fluid is supplied to the atomizer with a cotton stick here, in order to prevent short circuits of the electrodes on the piezoceramic ring. The equipment to be measured is shown in Fig. 8(b). The dispenser was kept a short distance to the cotton stick during this measurement. As effected by the water surface tension, a liquid bridge will be formed between the cotton stick and the dispenser. The liquid to be atomized is supplied with this liquid bridge.

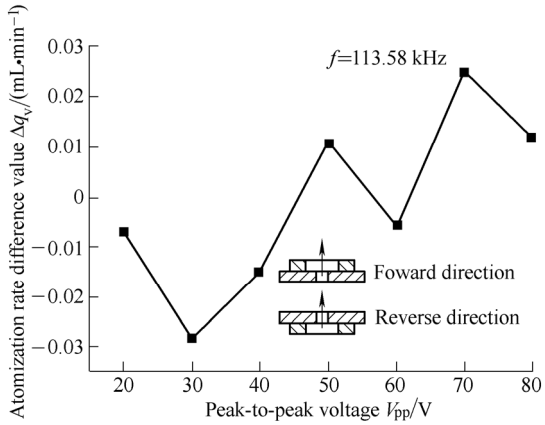


Fig. 10. Difference values of the atomizer rates of the micro straight aperture atomizer before and after the direction change

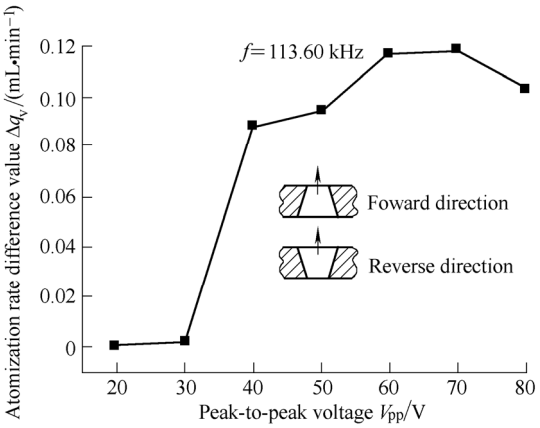


Fig. 11. Difference values of the atomizer rates of the micro-tapered aperture atomizer before and after the direction change

Fig. 10 shows the atomization rate difference values with the voltage at 113.58 kHz when the micro straight aperture atomizer is in the forward and reverse directions. As constrained by the processing method, the micro straight aperture with the same dimensions as the micro-tapered aperture is unavailable. The micro straight aperture with a diameter of about 100 μm is used in this letter.

The experiment illustrated in Fig. 10 shows that atomization can be generated under both forward and reverse directions when the voltage is from 20 V to about 40 V. When the voltage increases, the atomization rate also increases. However, as the voltage increases, the atomizer rates under the forward and reverse directions are basically the same and almost no atomizer rate difference value is caused.

Fig. 11 shows the atomization rate difference values

with the voltage at 113.60 kHz when the micro-tapered aperture atomizer is operating in the forward and reverse directions. It is found during the measurement that no visible atomization, instead only drops are observed at the micro-tapered aperture under the forward and reverse directions when the voltage is less than 30 V. For the micro-tapered aperture under the forward direction, visible atomization is generated when the voltage is higher than 30 V, and the atomization rate increases when the voltage increases. For the micro-tapered aperture under the reverse direction, only water drops are formed even when the voltage reaches 70 V. However, when the voltage is greater than 70 V and reaches 80 V, atomization begins. The atomization rate measured under the forward direction is much higher than that measured under the reverse direction. The atomization rate difference increases as the voltage increases. In the test described above, aperture directions are directly related to atomization conditions, and the micro-tapered aperture produces effects.

## 6 Conclusions

(1) In this letter, the dynamic cone angle effect on the atomization is proven theoretically. The volume of a micro-tapered aperture in the dispenser changes when the dispenser is vibrating. In the micro-tapered aperture, flows are observed in both nozzle and diffuser elements. As the flow resistances in the nozzle and diffuser elements are different, the flow rates in the nozzle and diffuser elements are also different, which allows the macroscopic flow from the flared side to the tapered side in the aperture. This is how the dynamic cone angle phenomenon drives the dispenser atomization.

(2) The pumping effect of the dynamic cone angle occurs only when the material of the dispenser has good elasticity, poor rigidity, or strong periodic force. The dispenser with micro-tapered apertures can be easily actuated by the high-frequency vibration of a piezoceramic ring. In this case, the dynamic tapered aperture enhances the pumping action while increasing the range of droplet sizes. This effect is commonly found in nozzles for high-pressure engines and printers that need smaller droplet sizes and lower dispersion. Reducing the dynamic tapered angle pumping effect may be an important endeavor to improve nozzles for high-pressure engines and printers.

(3) In the experiments, the atomizer rates of the atomizer with a micro straight aperture dispenser in the forward and reverse directions are almost the same, while the atomizer rates of the atomizer with a micro tapered aperture dispenser in the forward and reverser directions are significantly different. The difference value increases as the voltage increases. Also, it is found by measurements that the atomizer rate under each resonance point is connected with the degree, to which the cone aperture is deformed but independent on the degree, to which the dispenser is deformed. It is fully validated in these two experiments that the dynamic cone angle phenomenon drives the atomization. The atomizers with better performance are especially applicable in the fields including Inhalation therapy, nano-atomization dry, and so on.

## References

[1] CHETAN M, NEGOIAS A. New approaches to nebulizer drug delivery[C]//*Advanced Topics in Electrical Engineering (ATEE); 7th International Symposium on*, Bucharest, Romania, 2011: 1–4.

[2] FDA U. *Reviewer guidance for nebulizers, metered dose inhalers, spacers and actuators*[EB/OL]. (2014). http://www.fda.gov/medicaldevices/deviceregulationandguidance/guidancedocuments/ucm081282.htm.

[3] FORREST S R. The path to ubiquitous and low-cost organic electronic appliances on plastic[J]. *Nature*, 2004, 428(6986): 911–918.

[4] AHMAD Z, HUANG J, THIAN E S, et al. Freeform fabrication of nano-biomaterials using 3D electrohydrodynamic print-patterning [J]. *Journal of Biomedical Nanotechnology*, 2008, 4(2): 185–195.

[5] CHOI K H, ALI J, NA K-H. Fabrication of graphene-nanoflake/poly(4-vinylphenol) polymer nanocomposite thin film by electrohydrodynamic atomization and its application as flexible resistive switching device[J]. *Physica B: Condensed Matter*, 2015, 475: 148–155.

[6] MEMARZADEH K, SHARILI A S, HUANG J, et al. Nanoparticulate zinc oxide as a coating material for orthopedic and dental implants[J]. *Journal of Biomedical Materials Research Part A*, 2015, 103(3): 981–989.

[7] LEE S H, HENG D, NG W K, et al. Nano spray drying: a novel method for preparing protein nanoparticles for protein therapy[J]. *International Journal of Pharmaceutics*, 2011, 403(1–2): 192–200.

[8] QUISPE-CONDORI S, SALDAÑA M D A, TEMELLI F. Microencapsulation of flax oil with zein using spray and freeze drying[J]. *LWT-Food Science and Technology*, 2011, 44(9): 1880–1887.

[9] NANDIYANTO A B D, OKUYAMA K. Progress in developing spray-drying methods for the production of controlled morphology particles: From the nanometer to submicrometer size ranges[J]. *Advanced Powder Technology*, 2011, 22(1): 1–19.

[10] CARNÉ-SÁNCHEZ A, IMAZ I, CANO-SARABIA M, et al. A spray-drying strategy for synthesis of nanoscale metal–organic frameworks and their assembly into hollow superstructures[J]. *Nature Chemistry*, 2013, 5(3): 203–211.

[11] SANTANGELO P E, JACOBS B C, REN N, et al. Suppression effectiveness of water-mist sprays on accelerated wood-crib fires[J]. *Fire Safety Journal*, 2014, 70: 98–111.

[12] JENFT A, COLLIN A, BOULET P, et al. Experimental and numerical study of pool fire suppression using water mist[J]. *Fire Safety Journal*, 2014, 67: 1–12.

[13] ZHUO J, YINSHUI L, XUFENG Z, et al. A portable piston-type water mist fire extinguisher for spacecraft[J]. *Proceedings of the Institution of Mechanical Engineers, Part E: Journal of Process Mechanical Engineering*, 2015, 229(1): 52–63.

[14] DENG Dong, ZHOU Hua, YANG Huayong. Emulational and experimental study of new water mist spray nozzle for fire suppression[J]. *Chinese Journal of Mechanical Engineering*, 2006, 42(12): 122–127. (in Chinese)

[15] LU C F, FU C C, YANG J C, et al. 4A-3 traveling wave driven micro-dispenser for CPU cooling application[C]//*2006 IEEE Ultrasonics Symposium*, Vancouver, BC: IEEE, 2006: 54–57.

[16] HOU Y, TAO Y, HUAI X. The effects of micro-structured surfaces on multi-nozzle spray cooling[J]. *Applied Thermal Engineering*, 2014, 62(2): 613–621.

[17] NEGEED E-S R, HIDAKA S, KOHNO M, et al. Effect of the surface roughness and oxidation layer on the dynamic behavior of micrometric single water droplets impacting onto heated surfaces[J]. *International Journal of Thermal Sciences*, 2013, 70: 65–82.
[18] PANÃO M R O, MOREIRA A L N, DURÃO D F G. Thermal-fluid assessment of multijet atomization for spray cooling applications[J]. *Energy*, 2011, 36(4): 2302–2311.
[19] HEIJ B de, SCHOOT B van der, ROOIJ N F de, et al. Modelling and optimisation of A vaporiser for inhalation drug therapy[C]//*Technical Proceedings of the 1999 International Conference on Modeling and Simulation of Microsystems*, Puerto Rico, USA: NSTI, 1999: 542–545.
[20] DE HEIJ B, VAN DER SCHOOT B, BO H, et al. Characterisation of a fL droplet generator for inhalation drug therapy[J]. *Sensors and Actuators A: Physical*, 2000, 85(1–3): 430–434.
[21] PAN C T, SHIEA J, SHEN S C. Fabrication of an integrated piezo-electric micro-nebulizer for biochemical sample analysis[J]. *Journal of Micromechanics and Microengineering*, 2007, 17(3): 659–669.
[22] MAEHARA N, UEHA S, MORI E. Influence of the vibrating system of a multipinhole-plate ultrasonic nebulizer on its performance[J]. *Review of Scientific Instruments*, 1986, 57(11): 2870.
[23] MAEHARA N, UEHA S, MORI E. Optimum design procedure for multi-pinhole-plate ultrasonic atomizer[J]. *Japanese Journal of Applied Physics*, 1987, 26(S1): 215–217.
[24] SHEN S-C, WANG Y-J, CHEN Y-Y. Design and fabrication of medical micro-nebulizer[J]. *Sensors and Actuators A: Physical*, 2008, 144(1): 135–143.
[25] SHEN S C. A new cymbal-shaped high power microactuator for nebulizer application[J]. *Microelectronic Engineering*, 2010, 87(2): 89–97.
[26] LU C, YANG J, FU C. No back-pressure effect micro-dispenser suction pump[C]//*2006 International Microsystems, Package, Assembly Conference Taiwan*. Taipei: IEEE, 2006: 1–4.
[27] WHITE F M. *Fluid mechanics*[M]. New York: McGraw-Hill, 2003.
[28] OLSSON A, STEMME G, STEMME E. Numerical and experimental studies of flat-walled diffuser elements for valve-less micropumps[J]. *Sensors and Actuators A: Physical*, 2000, 84(1–2): 165–175.
[29] ZHANG Jianhui, XIA Qixiao, ZHEN Hong, et al. Flow direction of piezoelectric pump with nozzle/diffuser-elements[J]. *Chinese Journal of Mechanical Engineering*, 2004, 17(1): 107–109.

## Biographical notes

CAI Yufei, born in 1984, is currently a PhD candidate at *College of Aerospace Engineering, Nanjing University of Aeronautics and Astronautics, China.* His research interests include air vehicle environment control and atomization.
E-mail: locyfve@nuaa.edu.cn

ZHANG Jianhui, born in 1963, is currently a professor and a PhD candidate supervisor at *School of Electro-Mechanical Engineering, Guangzhou University, China.* His research area is mechanical design and its theory, piezoelectric driving.
E-mail: zhangjh@nuaa.edu.cn

ZHU Chunling, born in 1968, is currently a professor and a PhD candidate supervisor at *College of Aerospace Engineering, Nanjing University of Aeronautics and Astronautics, China.* Her research area is air vehicle environment control and aircraft de-icing/anti-icing calculation and design.
E-mail: clzhu@nuaa.edu.cn

HUANG Jun, born in 1981, is currently a PhD at *Research Center of Fluid Machinery Engineering and Technology, China.* His research area is piezoelectric driving, fluid solid coupling analysis and multi-field simulations.
E-mail: huangjun551@nuaa.edu.cn

JIANG Feng is a master graduate from *State Key Laboratory of Mechanics and Control of Mechanical Structures, Nanjing University of Aeronautics and Astronautics, China.* His research area is mechanical design and its theory, piezoelectric driving.
E-mail: yorkarthur@126.com